

# Design and testing of a fiber-coupled fast neutron scintillation detector for low-power research reactors

Alexis Dupont Bembinnoff<sup>1,\*</sup>, Oskari Pakari<sup>1,2</sup>, Daniel Clément<sup>1</sup>, Thomas Ligonnet<sup>1</sup>, Mathieu Hursin<sup>1,2</sup>, Andreas Pautz<sup>1,2</sup>, Vincent Lamirand<sup>1,2</sup>

<sup>1</sup>École Polytechnique Fédérale de Lausanne (EPFL), Switzerland

<sup>2</sup>Paul Scherrer Institut (PSI), Switzerland

(\*)[alexis.dupont-bembinnoff@epfl.ch](mailto:alexis.dupont-bembinnoff@epfl.ch)

**Abstract**—We present a new fiber-coupled organic scintillator fast neutron detector. Plastic scintillators are used in many applications to detect fast neutrons and gamma rays. The interest in small, fiber-coupled scintillation detectors is in their ability to perform high-resolution neutron flux measurements to ultimately provide multi-physics flux data in research nuclear reactors. Such measurements are planned in the framework of the EURATOM EVEREST project, specifically in the JSI-TRIGA and BME reactors to produce data for code validation.

A 5x5x5 mm EJ-276D scintillator was tested with and without optical fiber coupling to a PMT with Pu-Be and <sup>137</sup>Cs sources. The Pulse Shape Discrimination histograms with coupling were still showing a region of interest for neutron detection. We produced a prototype reactor sensor with a surface of 1 mm<sup>2</sup> (V=0.3 mm<sup>3</sup>) for high resolution experiments. The 0.3 mm<sup>3</sup> scintillators were coupled to a 20 m optical fiber for a set of experiments with a strong Co<sup>60</sup> (≈250 GBq) source and in the zero-power reactor CROCUS. The neutron detection capability was assessed in CROCUS for different power levels. The fiber-coupled small-sized scintillators have shown a linear response up to 25 W (total flux around 3.8x10<sup>8</sup> cm<sup>-2</sup>.s<sup>-1</sup>). Ongoing developments include testing alternative scintillation materials such as stilbene and organic glass. Future work will focus on experiments in the JSI-TRIGA reactor at higher neutron fluxes and smaller detector volumes.

**Index Terms**—Organic scintillator, fast neutron, detection, high-resolution, fiber-coupling, CROCUS, research reactor, photo-multiplier tube.

## I. INTRODUCTION

MODERN simulation codes for nuclear reactor neutronics can predict power with high spatial resolution, enabling the study of intra-fuel-pin neutron flux effects [1]. As part of the HORIZON-EURATOM-2023 initiative focused on advancing solutions for nuclear reactor pressure vessel aging and safety margin assessment, the EVEREST project (Experiments for Validation and Enhancement of the REactor preSSure vessel fluence assessmentT) is dedicated to the development of advanced multiphysics simulation tools for accurate prediction of neutron fluence in nuclear power plant reactor vessels. Tackling the multiphysics phenomena happening in a nuclear power plant could allow to optimize conventionally used conservative safety margins for the better, and therefore extend the lifetime of nuclear power plants. To validate these codes, we require measurements that are well and sufficiently localized (in between the fuel pins). The pursuit of cost-effective alternatives to miniature fission

chambers is important to facilitate the deployment of a larger number of detectors. To observe multiphysics phenomena, powers on the order of 50 kW need to be reached to observe temperature feedback in the reactors of interest [2], [3], [4], [5]. A key challenge is thus the development of new high-resolution neutron detectors capable of handling the associated fluxes, whilst being exposed to comparatively high gamma ray fluxes, relatively increased temperatures (in the range of 50°C), and perturbations such as coolant movement.

Small detectors are of particular interest for performing highly localized measurements in confined geometries, such as inter-pin regions. In this context, IPEN conducted such measurements in 2024 using TLD-100 detectors within the IPEN/MB-01 core [6]. Furthermore, intra-pin dosimetry carried out in the NECTAR experiments [7], [8], [9] at the CROCUS reactor demonstrated the feasibility of achieving highly localized neutron flux measurements using gold foils. However, passive detection does not provide feedback on phenomena leading to a temporal variation of the measured quantity (occurring on the timescale of one second), whereas an active detection system can.

An important avenue of development is the use of optical fiber-coupled neutron scintillation detectors. The light collection electronics are often large (~cm), and placing scintillators into reactors or other spatially constrained environments is therefore challenging or altogether impossible. By fiber-coupling a <1 mm scintillator to the light collection electronics (usually a SiPM or PMT), new measurement locations - both in terms of space and electronics sensitivity - could be unlocked.

Scintillator-based fiber-coupled detectors were previously developed at Nagoya University in 1994 by Mori et al. [10] and at EPFL in 2020 [11], [12], [13], [14]. The work done at EPFL showed that small inorganic scintillators (ZnS:LiF based) can be used for thermal neutron detection in a zero power research reactor [15]. The detectors show linear responses up to 6.5W (total flux of 7.7x10<sup>7</sup> cm<sup>-2</sup>.s<sup>-1</sup> and thermal flux of 3.2x10<sup>7</sup> cm<sup>-2</sup>.s<sup>-1</sup>). They are unsuitable for higher power (limitation in the electronic) or even multi-physics relevant experiments in the current design [16]. Other researchers developed small fast neutron fiber-coupled detection system with inorganic scintillators [17], [18]. Our work explores a new angle on organic fast neutron scintillator development. Organic scintillators were previously tested in CROCUS [19], [20], but only at lower powers (up to 50mW), as the PMT was

also in the reactor core.

In this article, we introduce a novel fast neutron detection system designed for high spatial resolution. The objective is to operate it in harsher environments than zero power reactors where multiphysics phenomena can be observed. The article is structured as follows: Section II introduce the different systems we use to develop the detector, section III presents the feasibility to perform Pulse Shape Discrimination (PSD). Section IV is dedicated to fiber-coupling neutron detection with an industrial sized scintillator (125 mm<sup>3</sup>). Moreover, this section deals with the size reduction of the scintillator to decrease the gamma sensitivity and perform neutron counting in the zero power reactor CROCUS at different power states. Finally, section IV summarizes the different capacities of different scintillator sizes.

## II. DESIGN OF THE FIBER-COUPLED ORGANIC FAST NEUTRON DETECTION SYSTEM

### A. Organic fast scintillators EJ-276D

The detector material used in this development is EJ-276D, manufactured by Eljen Technologies [21]. It is a plastic scintillator designed for gamma-ray and fast neutron detection. It has been characterized for neutron monitoring [22], [23], compared with other conventional detectors [24] or used for spectrometry purposes [25].

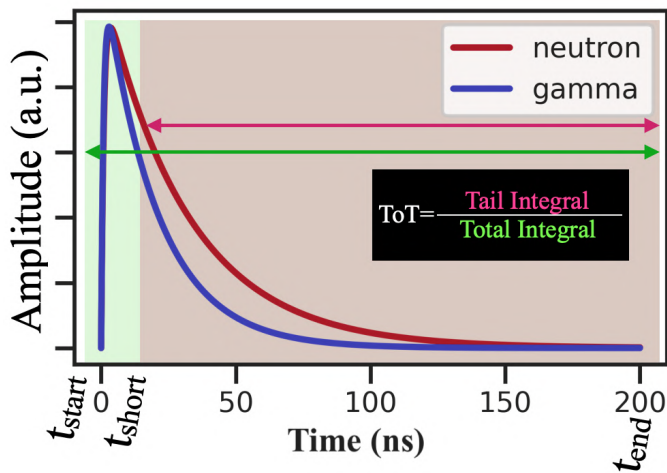


Fig. 1: Illustration of waveforms for neutron scintillation (in red) and gamma-ray scintillation (in blue) inside a PSD capable plastic scintillator.  $t_{short}$  (in green) is the starting time of the tail integration for calculating the ToT ratio

Gamma rays interact preferentially with the organic material via Compton scattering, leading to an electron causing scintillation. Neutron detection occurs through proton recoil interactions with hydrogen nuclei. Due to the much higher linear energy transfer (LET) of protons compared to electrons, the excited electronic states differ from those in gamma-ray induced scintillation. Higher energy states are reached, thus some electrons are jumping on triplet states back and forth inducing a longer decay shape as shown Figure 1. Neutron induced prompt fluorescence exhibits distinct *longer* decay times compared to gamma-ray interactions, enabling so-called Pulse Shape Discrimination (PSD) methods to classify pulses into gamma ray or neutron induced. Figure 1 illustrates the

difference in expected waveforms, highlighting the small but significant difference in fluorescence decay of some 30 ns [21].

In order to use this difference, the principle of PSD is based on calculating the Tail-over-Total (ToT) ratio (Fig. 1) of the pulse, as shown in Eq. (1). The integral of the tail for neutron interactions is larger than that for gamma-ray interactions, so the ratio between the tail integral and the total integral allows for the discrimination of these two particle types in a 2D clustering histogram.

$$ToT = \frac{\int_{t_{short}}^{t_{end}} S(t)dt}{\int_{t_{start}}^{t_{end}} S(t)dt} \quad (1)$$

Where  $S(t)$  is the signal wave function,  $t_{start}$  is the starting time of the wave,  $t_{end}$  is the ending time of the wave, and  $t_{short}$  is the starting time of the tail integration. From the ToT we can plot a 2D histogram so called Pulse Shape Discrimination plot (PSD plot) with in y-axis the ToT and x-axis the deposited energy (or energy). The PSD plot would show two separated clusters for a mixed field measurement ( $n+\gamma$ ): one for the neutron (higher ToT) and one for the gamma rays (lower ToT), and one peak for pure gamma-rays measurement corresponding to gamma scintillation detection. For the study, multiple scintillator sizes are investigated:

- 1) conventional 10 x 10 x 10 mm cube (1 cm<sup>3</sup>)
- 2) standard 5 x 5 x 5 mm cube (125 mm<sup>3</sup>)
- 3) custom cut 0.6 x 0.6 x 0.9 mm miniature scintillator (0.3 mm<sup>3</sup> mass based)

The latter 0.3 mm<sup>3</sup> scintillator is a piece manually cut at EPFL from a polished 5 x 5 x 5 mm<sup>3</sup> cube. To achieve this size, the cube was sawn while preserving a polished side. This piece was placed on modeling clay (Fig.2) for cutting and preventing the small parts to be projected somewhere else.



Fig. 2: Size of the first cut of EJ-276D scintillator (left), and picture of the modeling clay use to hold the piece in place for further cutting (right).

The small piece stuck in the modeling clay was then cut with a cutter multiple times to obtain a sub mm<sup>3</sup> scintillator with one side polished for the fiber coupling. The size reduction of the scintillator decreases the overall sensitivity of it. Previous reactor tests of organic scintillators revealed a volume-dependent effect on sensitivity [20].

### B. Optical fiber

The scintillators were coupled to polished PMMA optical fibers by ESKA [26], [27] of two diameters. For the two largest scintillator cubes, the fiber core had a diameter of 2 mm and a 1 mm jacket. For the smallest scintillator, the fiber core had a diameter of 1 mm and a 1.2 mm jacket. The refractive index of the core is 1.49, and coupling was improved by using EJ-550

optical silicone grease (refractive index: 1.46) manufactured by Eljen Technologies [21] to reduce scintillation photon loss from the fiber/scintillator interface.

For the 1 cm<sup>3</sup> and 125 mm<sup>3</sup> scintillators, an aluminum fiber-holder was used to ensure the fiber is perpendicular to the contact surface (see Figure 3). The holder is a 5×5×5 mm cube with a 3.1 mm diameter hole to accommodate the fiber. Black electrical tape was placed around the three components (scintillator, holder, and fiber) to secure them together, ensuring a mechanically stable system during transport. The 0.3 mm<sup>3</sup> scintillator was positioned at the tip of a fiber (also using optical grease) and protected with an aluminum cap (see Figure 3). Black electrical tape was then used to wrap and secure the cap to the fiber, preventing background light from entering.

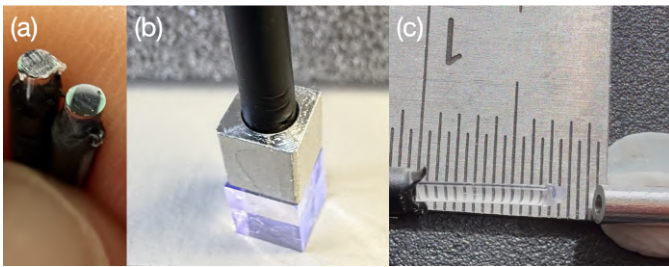


Fig. 3: (a) difference between a ground fiber (left) and a polished fiber (right) for scintillator and PMT coupling; (b) 125 mm<sup>3</sup> scintillator with aluminum holder on top holding the 3 mm diameter fiber; (c) 0.3 mm<sup>3</sup> scintillator on the tip of the 2.2 mm diameter fiber (left) before putting the aluminum cap (on the right).

### C. Photo-Multiplier Tube (PMT)

The used Photo-Multiplier Tube (PMT) is the H3178-51 model from Hamamatsu [28]. The PMT was powered with a bias voltage between 1.3 kV and 1.5 kV. The expected gain from the manufacturer datasheet is  $7.9 \times 10^5$ .

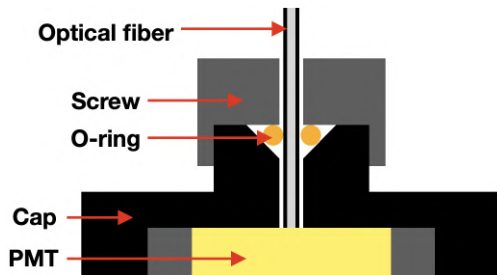


Fig. 4: Scheme of the fiber holder on top of the PMT with the screw and the O-ring for a sturdy and repeatable setup.

Depending on the experimental setup, either the scintillator or the fiber was coupled to the PMT using EJ-550 optical silicone grease to optimize scintillation photon transmission. For fiber coupling, the rear end of the fiber was attached to the PMT using an in-house developed screw holder (see Figure 4). The holder is essentially a black PVC cap with a thickness of 1 cm. It features a conical hole that houses an O-ring for gripping the fiber. When the screw is screwed to the cap, the O-ring is trapping the fiber. Thanks to this, the fiber is correctly held in the same position for each experiment and the background light is not interacting with the PMT photocathode.

### D. Data acquisition

The PMT signal was read by a 500 MS/s CAEN DT5730S digitizer [29]. The DPP-PSD CAEN firmware [30] was used for signal acquisition, real-time pulse shape discrimination (PSD), energy spectrum generation, and waveform plotting. A waveform is recorded only if its rising edge exceeded the trigger threshold set for the experiment (0.12 mV in our case). Table I presents the fixed settings of the digitizer used in all experiments. These settings were arbitrary set during the experiments to obtain the best PSD plot configuration.

TABLE I: Digitizer settings for measurements

Discriminator mode	Leading edge
Trigger hold off	1024 ns
Pre-trigger	96 ns
Record length	992 ns
DC offset	20.0 %

To obtain the PSD plot from the digitizer, we defined what the digitizer internally calls a total gate and a short gate, as presented in Section II-A. The short gate is used for tail integration, while the total gate performs the full signal integration. From this point onward, the system—scintillator, fiber, PMT, and digitizer—is referred to as miniature organic scintillation system (MOSS).

## III. RESULTS: ORGANIC SCINTILLATOR MEASUREMENTS WITHOUT FIBER COUPLING

### A. Gamma ray reference measurement with a Cs<sup>137</sup> source

The goal of this experiment was to observe the gamma-ray response of the scintillator coupled to the PMT and determine whether an energy calibration can be performed using a <sup>137</sup>Cs source, and to provide a baseline experiment to compare our later neutron experiments to.



Fig. 5: Experimental setup for gamma-ray detection with 5x5x5 mm EJ-276D scintillator coupled to a PMT (1.3 kV) in front of a 125 kBq <sup>137</sup>Cs source.

For these experiments, the 5x5x5 mm (125 mm<sup>3</sup>) scintillator was directly coupled to the PMT without a fiber. The <sup>137</sup>Cs source was placed in front of the system (contact with the PMT cap). The bias voltage applied on the PMT was 1.3 kV, the energy coarse gain was 10fC/LSBxVpp and the short gate was set at 120 ns and the total gate at 600 ns. The waveform begins rising at 96 ns (pre-trigger), and 30 ns is sufficient to capture the peak height. The tail integral is calculated from 120 ns to 600 ns to ensure accurate horizontal clustering. The manner in which we herein quantify the detector response is the so-called PSD plot. The PSD plot consists of a 2D histogram where the deposited energy is on the x-axis and the ToT on the y-axis.

Figure 6 shows the PSD plot resulting from the <sup>137</sup>Cs experiment. The PSD plot shows a single band in the range ToT = [0.15, 0.21]. This band corresponds to gamma rays emitted and interacting within the scintillator. At lower energies (below

150 keV), pile-up effects are observed. In addition to the PSD plot, the pulse height integral spectrum (Fig. 7) was used to perform an energy calibration by using the Compton edge at 476 keV (with 661.7 keV being the full energy of emission of  $^{137}\text{Cs}$  [31]).

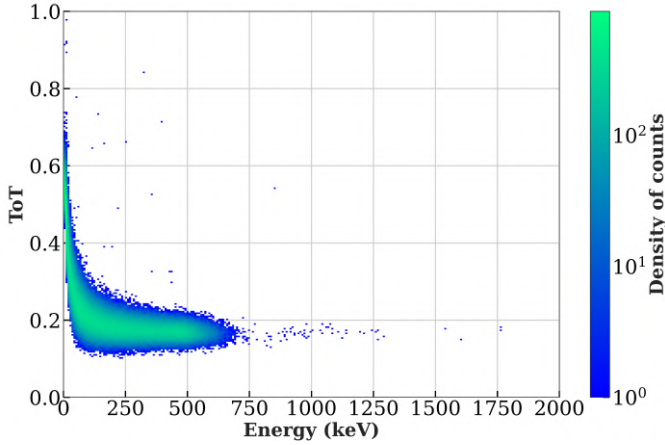


Fig. 6: Energy calibrated PSD plot of a 125 kBq  $^{137}\text{Cs}$  source measurement with a 125 mm<sup>3</sup> EJ-276D scintillator coupled to a PMT.

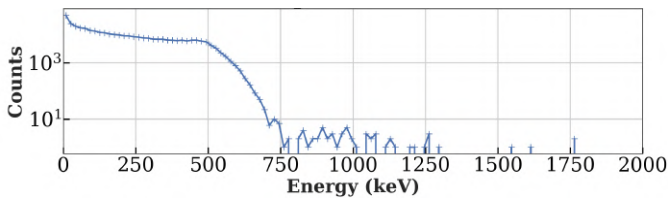


Fig. 7: Gamma ray energy spectrum for the 125 kBq  $^{137}\text{Cs}$  source measurement with a 125 mm<sup>3</sup> EJ-276D scintillator coupled to a PMT. Energy calibration was performed with the 475 keV Compton edge.

### B. Neutron and gamma-ray reference measurement with a PuBe source

The goal of this measurement was to test the detection of fast neutrons using Pulse Shape Discrimination (PSD), and establishing the optimal settings for distinguishing between the neutron and gamma contributions, i.e., the optimal choice for long and short gate settings.

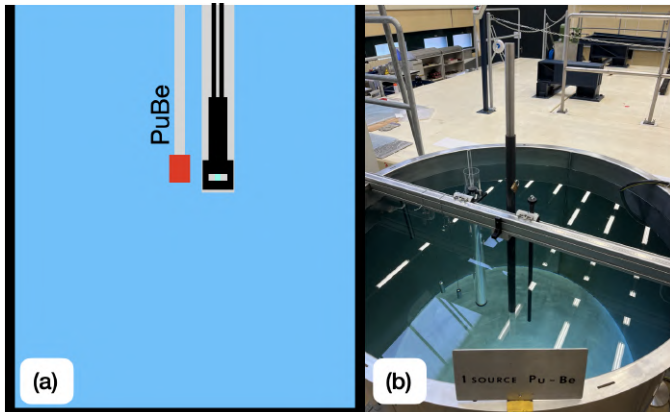


Fig. 8: (a) Setup of the mixed field (neutron & gamma-ray) irradiation in CARROUSEL with the 1 cm<sup>3</sup> EJ-276D scintillator coupled to a PMT with a bias voltage of 1.3 kV; (b) CARROUSEL facility with the PuBe source inserted in the central tube, and Plexiglass PMT holder tubes on its left and right sides.

We performed mixed field irradiation of the system with a Plutonium-Beryllium (PuBe) source in the CARROUSEL

facility. CARROUSEL is a cylindrical water tank that can hold a PuBe in its center [32], [15]. The PuBe source has an intensity of  $10^7 \text{ n.s}^{-1}$ .

For this experiment, the scintillator used was the 10x10x10 mm one (1 cm<sup>3</sup>). The PMT bias voltage was 1.3 kV and the optimized firmware settings are the same as section III-A: short integral 120 ns and total integral 600 ns. The PSD plot of the mixed-field measurement (Fig. 9) shows two distinct regions above few hundreds keV energy with different ToT values.

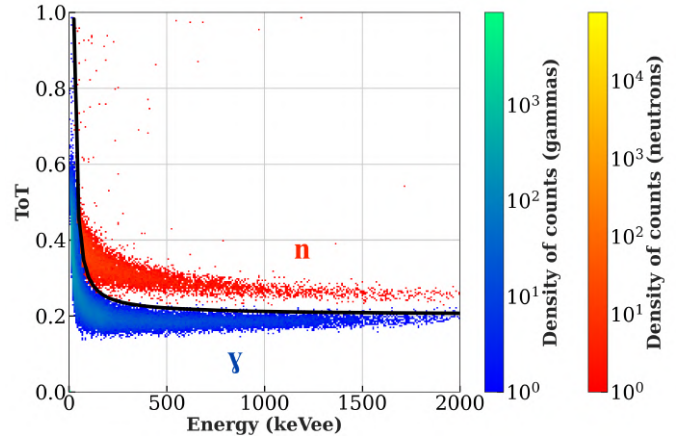


Fig. 9: Energy calibrated PSD plot with 1 cm<sup>3</sup> EJ-276D scintillator coupled to a PMT at 7 cm from a 185 GBq PuBe source with a PMT bias voltage of 1.3 kV. The detection events associated with neutrons are in red while the gamma ray detection events are in blue. The black line defines the discrimination limit.

According to the waveforms of the different scintillation processes, the red region of the plot corresponds to neutron detection, whereas the blue region corresponds to gamma-ray detection. For heavy charged particles (protons, in our case), the light yield per unit of energy is reduced compared to that for electrons [31], hence the y-axis in keVee (electron equivalent). The term keVee sets an absolute basis for the energy calibration.

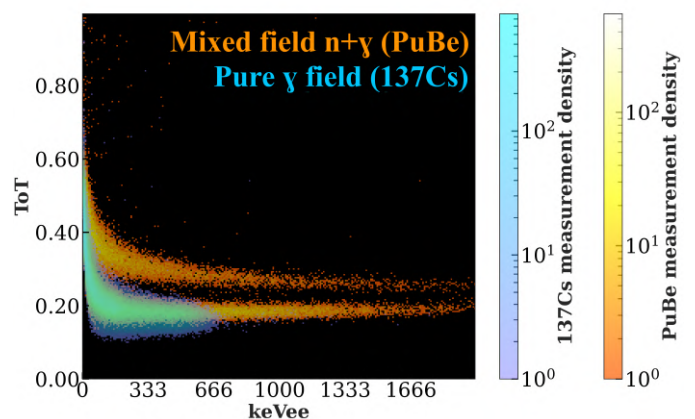


Fig. 10: PSD superposition between a mixed field neutrons & gamma ray (PuBe) PSD plot in orange-yellow and a pure gamma-ray field ( $\text{Cs}^{137}$ ) PSD plot in blue-green.

The low energy region (below 150 keV) smearing is due to pile-up phenomena. The black curve in Figure 9 delimits conservatively the decision threshold for gamma ray and neutron detection, i.e. we accept to misclassify some neutrons and in turn reduce the odds of misclassifying gamma rays.

To further illustrate that the red region in Figure 9 corresponds to neutron events, we introduce a PSD plot superposition in Figure 10 with a black background. From now on, PSD plots with black backgrounds will be PSD superposition plots (one in orange, one in blue). We observe that the peak from the previous pure gamma-ray measurement overlaps with the presumed gamma-ray peak in the mixed-field measurement. It is to be noted that it overlaps in the lower ToT peak of the PuBe measurements, which is expected considering the larger energy range of PuBe gamma rays. The gamma-ray region for this scintillator, with these settings, is in  $ToT=[0.15;0.21]$ .

#### IV. RESULTS: FIBER-COUPLED ORGANIC SCINTILLATOR

In this Section, we present our results with fiber-coupled organic scintillators, starting with irradiation of the medium-size one ( $125\text{ mm}^3$ ) in CARROUSEL, and finally the in-core test of the smaller one.

##### A. Mixed field and pure gamma-ray measurements with the $125\text{ mm}^3$ fiber-coupled scintillator

The first test consisted in irradiating the  $125\text{ mm}^3$  medium-size scintillator (for detection efficiency reasons) with the PuBe neutron and  $Cs^{137}$  gamma source successively, in order to replicate the analysis of Section III.

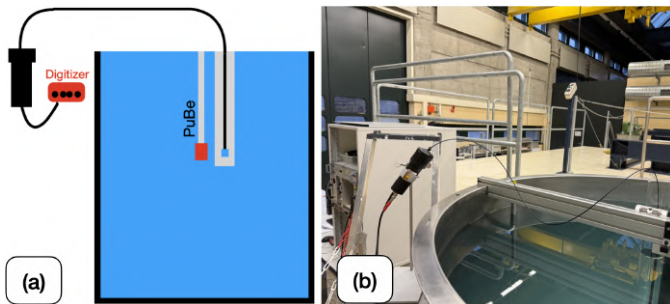


Fig. 11: (a) setup of the mixed field (neutron & gamma ray) detection in CARROUSEL with a  $125\text{ mm}^3$  scintillator (fiber of 2m, 1.5kV); (b) CARROUSEL facility with the PMT on a ladder and the optical fiber going into the experimental tube.

The scintillator was coupled to a 2m-long optical fiber (arbitrary length). As the coupling reduces the amount of scintillation light reaching the PMT, new digitizer settings are required for increasing the amplification. The PMT bias voltage was set to 1.5 kV, and the energy coarse gain was also adjusted to  $2.5\text{ fC/LSB}\times V_{pp}$ . The short gate and total gate are unchanged. The setup in CARROUSEL is presented in Figure 11.

The PSD superposition plot in Figure 12 shows the PuBe measurement (orange) with the previous setup and the  $^{137}Cs$  measurement (blue), similarly to Figure 10.

The coupling with the optical fiber changes the shape of peaks observed in the PSD plot. First, for the gamma irradiation, no Compton edge is observed, which is probably caused by the loss of scintillation photons at the different interfaces, and complicates energy calibration. From now on, the PSD plots with fiber coupling will be expressed in arbitrary deposited charges units.

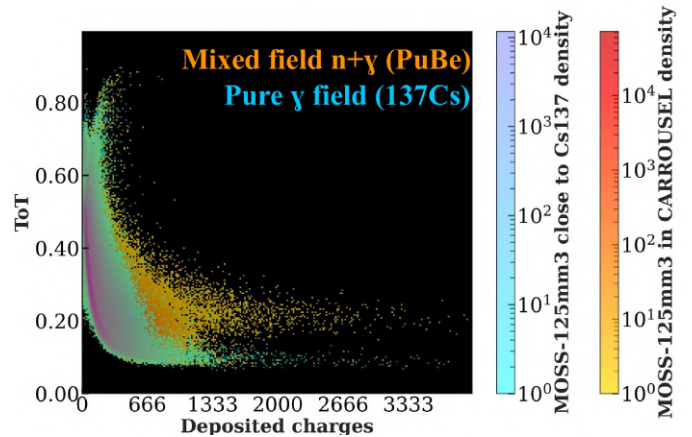


Fig. 12: Non energy calibrated PSD superposition plot between a  $125\text{ mm}^3$  scintillator (1.5 kV) with a 2m fiber in a neutron & gamma-ray mixed field in CARROUSEL (PuBe) and a pure gamma-ray field ( $^{137}Cs$ , 125 kBq) measurements

The two clusters present a globally larger mixed detection area. In the lower charge deposit region neutron detections, gamma-ray detection, and pile-up phenomena are overlapping. This is caused by the partial loss of photons in the fiber and the coupling, which broadens the PSD resolution due to pile-up effects. Nevertheless, two distinct regions corresponding to neutron and gamma-ray detections remain observable.

A major first conclusion is therefore that the fiber coupling still allows for discrimination between neutrons and gamma rays. The next step in our development is to reduce the size of the scintillator: first, to match the fiber size for a high-spatial-resolution system, and second, to reduce the number of overall detections per unit flux to increase operational range. Note that the smaller scintillator ( $0.3\text{ mm}^3$ ) showed a count rate too low (below background) with the PuBe source to allow for further characterization.

##### B. Measurement in CROCUS with the $0.3\text{ mm}^3$ fiber-coupled scintillator

The  $0.3\text{ mm}^3$  scintillator was tested under mixed field conditions in the zero-power reactor CROCUS. CROCUS is a light water moderated reactor, the criticality is controlled by the water level or with control rods. The neutron detection system, presented in the previous section, is inserted into the Southeast experimental air-channel of CROCUS, which consist of a guide tube with its control rod removed.

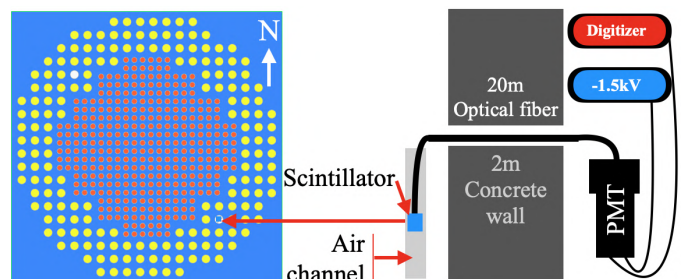


Fig. 13:  $0.3\text{ mm}^3$  scintillator measurement setup in CROCUS. The scintillator is placed in the middle of the South-East CROCUS control rod. A 20m fiber passes in the 2m concrete cavity wall and goes to the PMT and digitizer. This lattice was created with Honeycomb [33]

The goal of this experiment was to verify the PSD plot of a mixed field source with the 0.3 mm<sup>3</sup> scintillator as compared to the previous PuBe measurement with a larger volume detector. Additionally, we examined the scintillator neutron response with increasing power to assess linearity of counting.

The experiment involved data acquisition from reactor start-up up to 80W. Figure 15 shows the total PSD plot for the experiment in CROCUS. The PSD plot reveals a single cluster. The lower region of the plot is once again associated with gamma rays and pile-up phenomena.

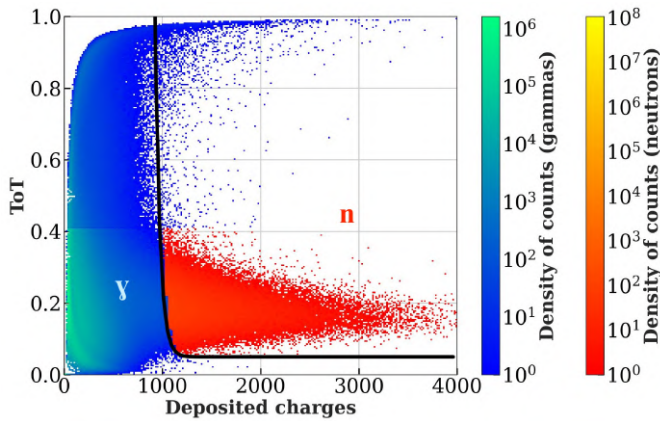


Fig. 14: Non-energy calibrated PSD plot for neutron & gamma ray mixed field in CROCUS with 0.3 mm<sup>3</sup> scintillator (bias voltage of 1.5 kV). The neutron events are in red while the gamma ray events are in blue.

We estimate, based on the mean free path of electrons in EJ276D, that individual gamma rays can only deposit up to 200 keV in the available volume of our smallest scintillator. Assuming that the neutrons transfer all their energy (average of 1-2 MeV in CROCUS [34]) to the proton, the energy deposited in the scintillator would be 2 MeV, based on proton energy loss mechanisms [35], [36], [37].

To further verify our hypothesis (neutron detection in the frame Figure 15), we performed an additional measurement conducted in the LOTUS cavity using the SILC Co<sup>60</sup> irradiator (source activity: 107 GBq as of 04.2025). This irradiation setup was previously found to be comparable to the gamma component of CROCUS [13], and allows for testing the gamma-ray energy deposits. The results are presented in Fig. 15.

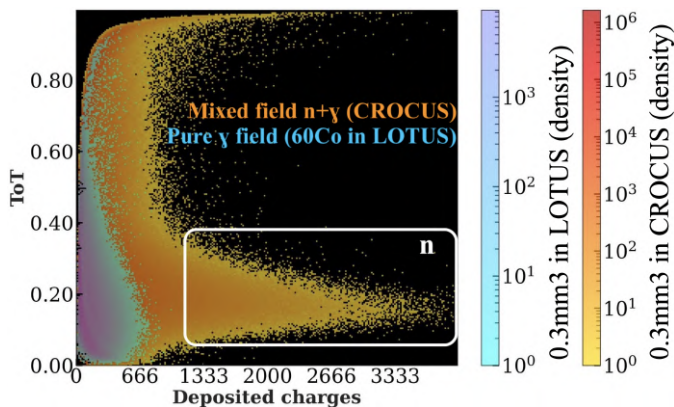


Fig. 15: PSD superposition between CROCUS measurement (in orange) and <sup>60</sup>Co (in blue) measurement with 0.3 mm<sup>3</sup> scintillator (bias voltages of 1.5 kV). The white frame corresponds to the neutron detection area for power monitoring.

Even if the gamma energy spectrum of Co<sup>60</sup> is relatively lower than the gamma spectrum in CROCUS, we estimated that the gamma-ray source gave us sufficient complementary information. Consequently, the single cluster was attributed to neutron detection only, corresponding to the white frame in Fig.15.

Finally, we performed a comparison between the 0.3 mm<sup>3</sup> scintillator neutron detection (i.e., events selected from the white frame shown in the PSD plot) and the CROCUS monitoring fission chamber n<sup>o</sup>2 from 80W power to shutdown. For the ease of comparison, the two signals were normalized to the average count rate during the 80W stabilization at criticality.

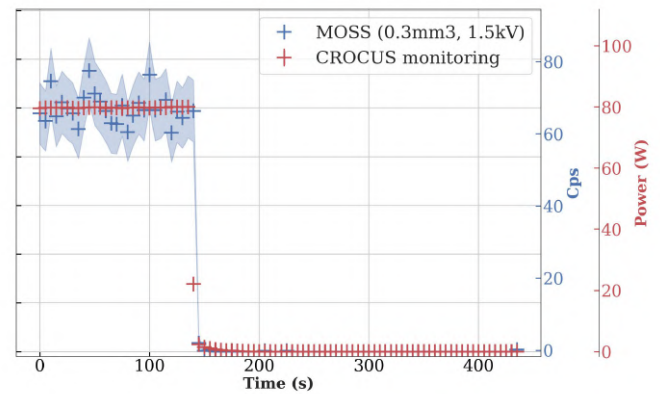


Fig. 16: Power tracking comparison between 0.3 mm<sup>3</sup> scintillator (1.5 kV) and CROCUS monitoring fission chamber n<sup>o</sup>2 during a shut-down from 80W to sub-critical. The dwell time of the two detectors is 5s.

According to previous research [38], [39], after shutdown, the delayed gamma-ray background in CROCUS corresponds to about 30% of the counts observed at 80W. Figure 16 displays the results from the shutdown measurement. The 0.3 mm<sup>3</sup> scintillator accurately follows the fission chamber profile, and does not plateau at 30% as would be expected with delayed gamma-rays. This provides further evidence that the white frame region corresponds to pure neutron counts.

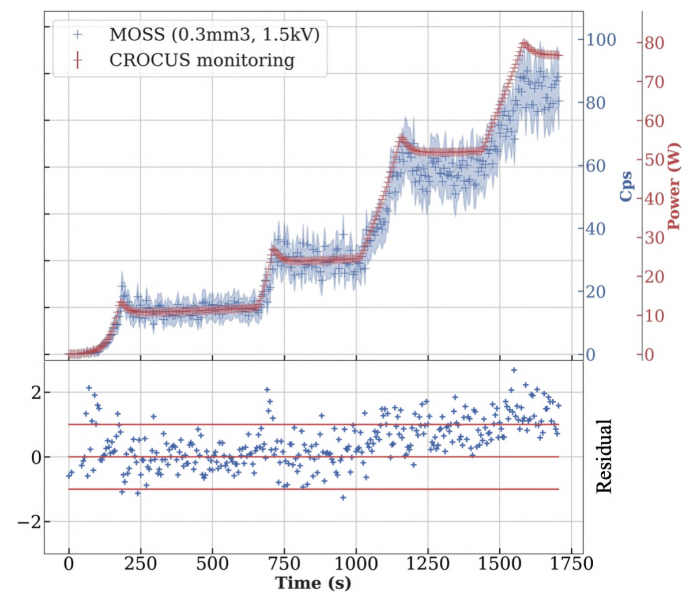


Fig. 17: Power steps comparison between the repetition of the 0.3 mm<sup>3</sup> fiber-coupled scintillator and CROCUS monitoring fission chamber n<sup>o</sup>2 during different power steps from 0 to 80W. Dwell time of the two detectors is 5s.

In addition to this measurement, we created a repetition of the previous detector (same volume of the scintillator) and performed a measurement of 4 different power steps in CROCUS (Fig.18).

The detector response is in agreement with the fission chamber (within 1 sigma) up to 25 W. However, above 25 W we observe a significative difference which is probably caused by the overloading of the digitizer with non neutron events (pile-ups). Future test will be carried out with an energy cut-off to prevent this overloading. Following these tests, monitoring was performed at different power levels in CROCUS to observe the detectors' behavior for a variety of scintillator sizes, and especially linearity, as shown in Figure 18).

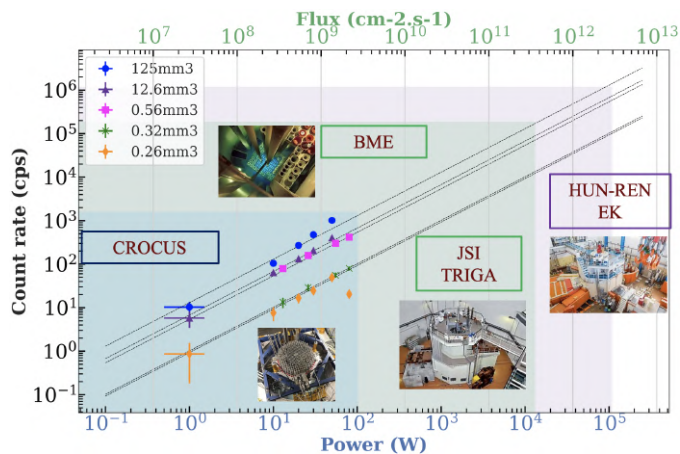


Fig. 18: Count rates of different sizes of scintillators as a function of power and flux in CROCUS South-East experimental channel. The colored regions correspond to the reactors' accessible neutron fluxes.

We tested different sizes of scintillator for the power steps experiment, each coupled to a 20m fiber. They all followed a linear trend with power/flux up to 25W. At higher power levels, the two biggest scintillators (125 mm<sup>3</sup> and 12.6 mm<sup>3</sup>) have shown an increase of the count rate. It is possibly caused by the misclassifications of gamma-ray events as neutron events. We can't solve this problem for the 125 mm<sup>3</sup> scintillators but for the 12.6 mm<sup>3</sup> we can change the neutron characterization window.

The 0.32 mm<sup>3</sup> and 0.6 mm<sup>3</sup> detectors were showing a very small decrease. We cannot definitively conclude the cause of this decrease. One possibility is the high data throughput in the electronics not keeping up with the signal (as we record all events, including pileups and other gamma ray events) or because the scintillation light is too intense and saturates the system, making it difficult to distinguish neutrons from pile-ups and gamma rays. All the measurements are taken into account for the linear fitting in Figure 18. Finally, a decrease in the count rate is observed for the smallest detector (0.26 mm<sup>3</sup>). It is caused by an experimental error and is not taken into account in the fitting. The smallest scintillators appear to be well-suited for the high-power experiments in other reactors within the EVEREST project. The maximum count rate readable by the CAEN digitizer is around 10<sup>6</sup>cps. With appropriate threshold settings we could therefore extrapolate a measurement capability up to a flux of 10<sup>12</sup>-10<sup>13</sup> n.cm<sup>-2</sup>.s<sup>-1</sup>. Naturally, this extrapolation is likely to not hold once tem-

peratures, Cherenkov light and mechanical vibrations in the higher-power reactors become significant (some 10 kW and above), and we plan to explore the neutron detection system behavior carefully to find the true limits.

## V. CONCLUSION

In this paper we present the development of fiber-coupled organic scintillators for fast neutron detection. Through Pulse Shape Discrimination, we established two distinct zones: one for neutron events and another for gamma-ray events. EJ-276D scintillator (125 mm<sup>3</sup> size) was coupled via an optical fiber to a PMT and irradiated in a mixed neutron and gamma-ray field. Despite the incurring light loss from fiber coupling, the detector still successfully performs pulse shape discrimination, and therefore neutron detection.

A final detection device was created with a 0.3 mm<sup>3</sup> scintillator to achieve the miniature size for high-resolution measurements in research reactors. Experiments were performed in the CROCUS zero-power reactor. By producing PSD superposition plots, we confirmed that the cluster associated with neutrons was indeed due to neutron-induced events. Power monitoring and comparison with the reactor shut-down from 80W was furthermore used to validate our hypothesis. In addition to that, we can assess that the detectors can operate up to 80W. By doing a repetition of the system with a second scintillator of the same volume, we were able to reach 80W with in agreement with the fission chamber measurement. For different volumes of scintillator we assessed the linearity of counting with increasing reactor power. By extrapolation, we provide a first hint at the feasibility of these fiber-coupled scintillators to provide data in higher fluxes reactors (10<sup>12</sup>-10<sup>13</sup> n.cm<sup>-2</sup>.s<sup>-1</sup>) performing high-spatial-resolution neutron detection.

Future work includes tests in research reactors at higher power levels, namely the JSI-TRIGA and BME reactors within EVEREST, in preparation of high resolution multiphysics experiments. We plan to also compare the performance of PMTs with Silicon Photomultipliers (SiPMs) for fiber coupling. Additionally, fiber coupling with other organic scintillator such as stilbene and Organic Glass Scintillator (OGS) developed at Michigan University are in preparation.

## AUTHOR'S CONTRIBUTION

Alexis Dupont Bembinoff, Oskari Pakari and Vincent Lamirand conceived, planned and carried out the experiments and the analysis. Alexis Dupont Bembinoff produced the analysing scripts, the scintillators-fiber couplings and the scintillator reduction. Daniel Clément handcrafted the PMT caps and fiber holders. Oskari Pakari is the head of nuclear facilities. Vincent Lamirand is the program manager of experimental research. Thomas Ligonnet helped for the data analysis. Mathieu Hursin is responsible for the EPFL contribution in the EVEREST project. Andreas Pautz is the head of the laboratory.

## ACKNOWLEDGMENT

The authors would like to thank the CROCUS operation team for their help and patience during the measurement

campaigns. The first author expresses his gratitude to Michel Saliba for his valuable guidance and insightful explanations, which enhanced his understanding of Pulse Shape Discrimination.

This project has received funding from the Horizon-Euratom Research and Training Program 2021–2027 through the EVEREST project under grant agreement n°101163288. Views and opinions expressed in this paper reflect only the authors' view, and the Commission is not responsible for any use that may be made of the information it contains.

## REFERENCES

- [1] M. Pecchia, H. Ferroukhi, A. Vasiliev, and P. Grimm, "Studies of intra-pin power distributions in operated bwr fuel assemblies using mcnp with a cycle check-up methodology," *Annals of Nuclear Energy*, vol. 129, pp. 67–78, 7 2019.
- [2] A. S. Ványi, B. Babcsányi, Z. I. Böröczki, A. Horváth, M. Hursin, M. Szieberth, and S. Czifrus, "Steady-state neutronic measurements and comprehensive numerical analysis for the bme training reactor," *Annals of Nuclear Energy*, vol. 155, 6 2021.
- [3] A. S. Ványi, M. Hursin, and S. Czifrus, "Analysis of transient measurements with thermal feedback and coupled trace/parcs calculations performed on the bme training reactor," *Annals of Nuclear Energy*, vol. 194, 12 2023.
- [4] V. Valero, L. Ottaviani, A. Lyoussi, V. Radulović, L. Snoj, A. Volte, M. Carette, and C. Reynard-Carette, "Thermal simulations of a new sic detector design for neutron measurements in jsi nuclear research reactor," in *Materials Science Forum*, vol. 1062 MSF, pp. 619–626, Trans Tech Publications Ltd, 2022.
- [5] H. Carcreff, V. Radulović, D. Fourmentel, K. Ambrožič, C. Destouches, L. Snoj, and N. Thiollay, "Nuclear heating measurements for fusion and fission relevant materials in the jsi triga reactor," *Fusion Engineering and Design*, vol. 179, 6 2022.
- [6] T. A. Cavalieri, P. de Tarso Dalledone Siqueira, J. M. B. Shorto, and H. Yoriyaz, "Thermal neutron dose measurements using tld-100 detectors in the ipen/mb-01 reactor core," *Applied Radiation and Isotopes*, vol. 208, p. 111302, 6 2024.
- [7] T. Mager, J.-B. Valentin, V. Lamirand, T. Ligonnet, W. D. Shin, J.-M. Fürbringer, M. Hursin, and A. Pautz, "Design of an instrumented fuel rod for intra-pin neutron flux measurements in the crocus experimental reactor," *EPJ Web of Conferences*, vol. 288, p. 04007, 2023.
- [8] T. Mager, O. Pakari, M. Hursin, T. Ligonnet, A. Pautz, and V. Lamirand, "Intra-pin reaction rate measurements in the crocus experimental reactor," *IEEE Transactions on Nuclear Science*, vol. 71, pp. 1047–1055, 5 2024.
- [9] T. Mager, M. Hursin, K. Vaughn, S. Choi, B. Kochunas, T. Ligonnet, V. Lamirand, O. Pakari, C. Fiorina, and A. Pautz, "Comparison of high-fidelity transport code predictions against the nectar intra-pin reaction rate measurements," *Annals of Nuclear Energy*, vol. 219, 9 2025.
- [10] C. MORI, T. OSADA, K. YANAGIDA, T. AOYAMA, A. URITANI, H. MIYAHARA, Y. YAMANE, K. KOBAYASHI, C. ICHIHARA, and S. SHIROYA, "Simple and quick measurement of neutron flux distribution by using an optical fiber with scintillator," *Journal of Nuclear Science and Technology*, vol. 31, pp. 248–249, 1994.
- [11] F. Vitullo, "Miniature and minimalistic neutron detectors for online high-resolution experiments in the zero-power reactor crocus," tech. rep.
- [12] F. Vitullo, V. Lamirand, K. Ambrožič, L. Braun, D. Godat, P. Frajtag, and A. Pautz, "Design of a 150-miniature detectors 3d core-mapping system for the crocus reactor," *EPJ Web of Conferences*, vol. 253, p. 04023, 2021.
- [13] F. Vitullo, V. Lamirand, J. B. Mosset, P. Frajtag, O. Pakari, G. Perret, and A. Pautz, "A mm3 fiber-coupled scintillator for in-core thermal neutron detection in crocus," *IEEE Transactions on Nuclear Science*, vol. 67, pp. 625–635, 4 2020.
- [14] M. Saliba, V. Lamirand, W. Monange, F. Vitullo, M. Hursin, A. Pautz, and O. Pakari, "Measurement of the prompt neutron decay constant in a zero-power reactor using a novel 3d detector system," 2025.
- [15] F. Vitullo, V. Lamirand, J.-B. Mosset, P. Frajtag, O. Pakari, P. Gregory, and A. Pautz, "Developing and testing a miniature fiber-coupled scintillator for in-core neutron counting in crocus," *EPJ Web of Conferences*, vol. 225, p. 04018, 2020.
- [16] C. Rochat, "Extension of miniature neutron scintillators features in crocus: novel acquisition scheme and extended flux range," jul 2021.
- [17] T. Yagi, T. Misawa, C. H. Pyeon, and S. Shiroya, "A small high sensitivity neutron detector using a wavelength shifting fiber," *Applied Radiation and Isotopes*, vol. 69, pp. 176–179, 1 2011.
- [18] T. Yagi, H. Unesaki, T. Misawa, C. H. Pyeon, S. Shiroya, T. Matsumoto, and H. Harano, "Development of a small scintillation detector with an optical fiber for fast neutrons," *Applied Radiation and Isotopes*, vol. 69, pp. 539–544, 2 2011.
- [19] F. B. Darby, O. V. Pakari, M. Y. Hua, V. Lamirand, S. D. Clarke, A. Pautz, and S. A. Pozzi, "Neutron-gamma noise measurements in a zero-power reactor using organic scintillators," *IEEE Transactions on Nuclear Science*, vol. 71, no. 5, pp. 1033–1040, 2024.
- [20] O. V. Pakari, A. Lucas, F. B. Darby, V. P. Lamirand, T. Maurer, M. G. Bisbee, L. R. Cao, A. Pautz, and S. A. Pozzi, "Gamma-ray spectroscopy in low-power nuclear research reactors," *Journal of Nuclear Engineering*, vol. 5, pp. 26–43, 1 2024.
- [21] E. Technologies, "<https://eljentechnology.com/products/plastic-scintillators/ej-276>."
- [22] K. D. Ngo, C. Cazzaniga, M. Paoletti, D. Rigamonti, M. Kastriotou, C. Frost, M. Tardocchi, J. Sykora, S. Mann, B. Lutz, and R. Nolte, "Fast neutron response characterization of an ej-276 plastic scintillator for use as a neutron monitor," *Nuclear Instruments and Methods in Physics Research Section A: Accelerators, Spectrometers, Detectors and Associated Equipment*, vol. 1051, p. 168216, 6 2023.
- [23] E. V. Ryabeva, I. V. Urupa, E. E. Lupar, V. V. Kadilin, A. V. Skotnikova, Y. A. Kokorev, and R. F. Ibragimov, "Calibration of ej-276 plastic scintillator for neutron-gamma pulse shape discrimination experiments," *Nuclear Instruments and Methods in Physics Research, Section A: Accelerators, Spectrometers, Detectors and Associated Equipment*, vol. 1010, 9 2021.
- [24] P. Pant, K. Banerjee, P. Roy, R. Shil, and A. K. Saha, "Characterization of ej-276d plastic scintillator and its comparison with ej-299-33a and bc-501a," *Journal of Instrumentation*, vol. 19, 10 2024.
- [25] E. V. Ryabeva, D. A. Molodtsev, I. V. Urupa, R. F. Ibragimov, V. V. Gaganov, E. E. Lupar, I. S. Vershinin, and D. I. Savin, "Ej-276 based neutron spectrometer with neutron-gamma pulse shape discrimination capability," *Nuclear Instruments and Methods in Physics Research Section A: Accelerators, Spectrometers, Detectors and Associated Equipment*, vol. 1034, p. 166791, 7 2022.
- [26] Mitsubishi, "<https://fiberfin.com/product/ff-sh-8001-3-0/>"
- [27] Mitsubishi, "Sh-4001 - ff-sh-4001-data-sheet."
- [28] Hamamatsu, "Photomultiplier tube assembly h3178-51."
- [29] CAEN, "Dt5730 / dt5730s 8 channel 14 bit 500 ms/s digitizer," 2024.
- [30] CAEN, "Compass multiparametric daq software for physics applications caen tools for discovery user manual um5960," tech. rep., 7 2024.
- [31] G. F. Knoll, *Radiation Detection and Measurement, 3rd ed.* John Wiley and Sons, 3rd edition ed., 2000.
- [32] E. L. Brunetto, F. Vitullo, V. Lamirand, K. Ambrožič, D. Godat, M. Buck, G. Pohlner, J. Starfinger, and A. Pautz, "High resolution measurements with miniature neutron scintillators in the sur-100 zero power reactor," *EPJ Web of Conferences*, vol. 253, p. 04029, 2021.
- [33] T. Guilbaud, "Honeycomb, an effective web tool to visualize and edit lattices," No. 1 in Transactions of the American Nuclear Society; 130, p. 1052–1053, American Nuclear Society, 2024.
- [34] A. Laureau, A. Gruel, V. Lamirand, T. Ligonnet, A. Sardet, A. Pautz, and al Analysis, "Analysis of the preliminary campaign for the petale program," *EPJ Nuclear Sci. Technol.*, vol. 9, p. 25, 2023.
- [35] A. Bozkurt, "Monte carlo calculation of proton stopping power and ranges in water for therapeutic energies," in *EPJ Web of Conferences*, vol. 154, EDP Sciences, 9 2017.
- [36] Z. Francis, S. Incerti, M. Karamitros, H. N. Tran, and C. Villagrasa, "Stopping power and ranges of electrons, protons and alpha particles in liquid water using the geant4-dna package," *Nuclear Instruments and Methods in Physics Research Section B: Beam Interactions with Materials and Atoms*, vol. 269, pp. 2307–2311, 10 2011.
- [37] B. W. Wiggins, A. Favalli, M. L. Iliev, K. D. Ianakiev, and M. P. Hehlen, "Computational investigation of arranged scintillating particle composites for fast neutron detection," *Nuclear Instruments and Methods in Physics Research, Section A: Accelerators, Spectrometers, Detectors and Associated Equipment*, vol. 915, pp. 17–23, 1 2019.
- [38] O. Pakari, T. Mager, V. Lamirand, P. Frajtag, and A. Pautz, "Delayed gamma fraction determination in the zero power reactor crocus," *EPJ Nuclear Sciences and Technologies*, vol. 7, 2021.
- [39] M. Hursin, C. Weiss, P. Frajtag, V. Lamirand, G. Perret, P. Kavrigin, A. Pautz, and E. Griesmayer, "Testing of a scvd diamond detection system in the crocus reactor," *European Physical Journal A*, vol. 54, 5 2018.